Appl Phys B (2012) 106:197–209
DOI 10.1007/s00340-011-4737-3

Applied Physics B
Lasers and Optics

Growth and characterization of Nd-doped disordered $Ca_3Gd_2(BO_3)_4$ crystal

Z.B. Pan · H.J. Zhang · H.H. Yu · M. Xu · Y.Y. Zhang · S.Q. Sun · J.Y. Wang · Q. Wang · Z.Y. Wei · Z.G. Zhang

Received: 7 March 2011 / Revised version: 29 June 2011 / Published online: 12 October 2011

Abstract A high-quality disordered Nd^{3+}:$Ca_3Gd_2(BO_3)_4$ (Nd^{3+}:CGB) laser crystal was grown by the Czochralski method. The space group and effective segregation coefficient of Nd^{3+} were determined to be *Pnma* and 1.06, respectively. The thermal properties, including the average linear thermal expansion coefficient, thermal diffusivity, specific heat, and thermal conductivity were systematically measured for the first time. It was found that the thermal conductivity increases with increasing temperature, indicating glasslike behavior. The polarized spectral properties of the crystal were investigated, including the polarized absorption spectra, polarized fluorescence spectra, and fluorescence decay. The spectroscopic parameters of Nd^{3+} ions in Nd^{3+}:CGB crystal have been obtained based on Judd–Ofelt theory. The anisotropy of the spectral properties for different polarized directions was discussed. Additionally, the continuous-wave (CW) laser performance at 1.06 μm was demonstrated for the first time. The maximum output power of 603 mW was achieved with corresponding optical conversion efficiency of 8.33% and slope efficiency of 9.95%.

Z.B. Pan · H.J. Zhang (✉) · H.H. Yu · M. Xu · Y.Y. Zhang · S.Q. Sun · J.Y. Wang
State Key Laboratory of Crystal Materials and Institute of Crystal Materials, Shandong University, Jinan 250100, People's Republic of China
e-mail: hjzhang@icm.sdu.edu.cn
Fax: +86-531-88574135

S.Q. Sun
Department of Physics, Shandong University, Jinan, Shandong 250100, People's Republic of China

Q. Wang · Z.Y. Wei · Z.G. Zhang
Institute of Physics, Chinese Academy of Sciences, Beijing 100190, People's Republic of China

1 Introduction

In the recent years, much work has been focused on the exploration of new solid state laser materials for efficient and compact high energy ultrafast laser sources. Up to now, the crystals with disordered structure are widely investigated due to the characteristics such as inhomogeneously broadening emission and absorption spectrum in combination with good thermomechanical properties, which are promising for generating ultrafast pulses [1–4].

Recently, a new disordered borate family with the formula $M_3Re_2(BO_3)_4$ (M = Ca, Sr, Ba; Re = Y, La, Gd) [5–7] have attracted a great deal of attention. The growth and spectral properties of Nd^{3+}-doped $M_3Re_2(BO_3)_4$ (M = Ca, Sr, Ba; Re = Y, La, Gd) were investigated [8, 9], which show that Nd^{3+}:$M_3Re_2(BO_3)_4$ can be grown by the Czochralski method and the absorption and emission spectra are strongly inhomogeneously broadened due to its disordered structure. This feature of broad spectra facilitates efficient pumping and production of ultrashort pulses [10, 11].

Nd^{3+}:$Ca_3Gd_2(BO_3)_4$(Nd^{3+}:CGB) is a member of Nd^{3+}-doped $M_3Re_2(BO_3)_4$. In this crystal, Ca^{2+} and Gd^{3+} ions are statistically situated in three different sites in the Nd^{3+}:CGB crystal structure [12], producing a disordered structure and large inhomogeneous broadening in the spectrum. Though the crystal has already been studied for several years, many basic but important properties such as the thermal and laser ones, have not been systematically characterized up to now.

In this paper, we report the thermal properties, including the average linear thermal expansion coefficient, thermal diffusion coefficient, specific heat, and thermal conductivity of Nd^{3+}:CGB for the first time to our knowledge. In addition, its spectral parameters, including polarized absorption and polarized emission spectra were studied by experiments and theory. The laser output at 1.06 μm with laser

diode (LD) pumping was obtained with the maximum output power of 603 mW.

2 Crystal growth

Since Nd^{3+}:CGB crystal melts congruently, Nd^{3+}:CGB can be grown by Czochralski method. The initial charge for growing single crystal was made from the raw materials $CaCO_3$, H_3BO_3, Gd_2O_3, and Nd_2O_3 with purity of 99.99%. The raw materials of Nd^{3+}:CGB were synthesized by the solid-state reaction according to the following chemical reaction equation:

$$6Ca_2CO_3 + 8H_3BO_3 + 1.99Gd_2O_3 + 0.01Nd_2O_3 = 2Ca_3Gd_{1.99}Nd_{0.01}(BO_3)_4 + 12H_2O\uparrow + 6CO_2\uparrow$$

The stoichiometric amounts of raw materials were weighed and combined. An excess quality of 3 wt% H_3BO_3 was added to compensate for the evaporation of B_2O_3 during growth [13]. Then the mixtures were grounded, mixed, and heated in a platinum (Pt) crucible at 900°C for 7 h in order to eliminate the absorbed water in the materials and decompose the carbonate. After the crucible cooled down to room temperature, the mixture was again grounded, mixed, pressed into cylinders under high pressure, and reheated at 1100°C for 10 h to prepare a Nd^{3+}:CGB polycrystalline material used for the single crystal growth through the solid-state reaction.

A Nd^{3+}:CGB single crystal was grown by the Czochralski method using a platinum (Pt) crucible in air atmosphere. The heating apparatus is a 2 kHz low radio-frequency furnace that was used to heat the crucible. Usually, in order to emit the bubbles in the melt and avoid the formation of the polycrystal in the crystal growth process, a temperature of 30–50°C higher than its melting point was required [14]. The temperature was held at that point for about 2–3 hours, and then lowered down to the melting point after dipping the seed into the melt and adjusting the heating power of the furnace. The Nd^{3+}:CGB crystal begins pulling at a rate of 0.5–0.8 mm/h, with the rotating rate of 10–15 rpm. After the crystal growth process, the crystal was cooled to room temperature at a rate of 15–30°C/h. The as-grown Nd^{3+}:CGB crystals have an excellent quality (no scatter pellets can be observed under 5 mW green laser). Figure 1 is the photograph of the as-grown Nd^{3+}:CGB crystal boule along the b direction. Its dimensions are about $\Phi 20 \times 25$ mm^2 and its mass is 52 g.

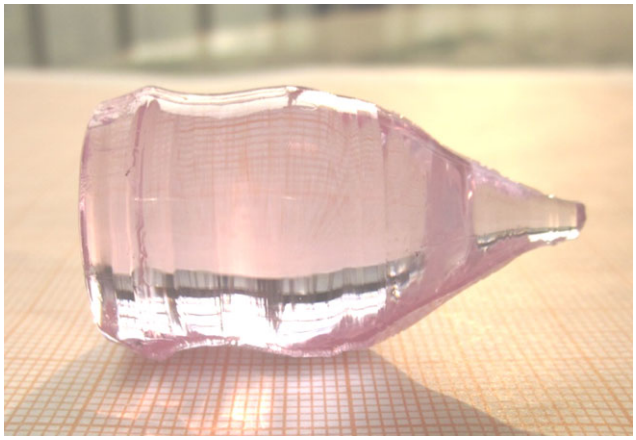

Fig. 1 0.5 at.% Nd^{3+}:CGB crystal grown along the *b*-direction

3 Experiment details

3.1 X-ray powder diffraction analysis

X-ray powder diffraction (XRPD) was performed to determine the lattice structure and lattice parameters of the as-grown Nd^{3+}:CGB crystal at room temperature. The crystal was grounded into powder for examination with an X-ray powder diffractometer (Bruker, model: Smart PPEX II) using the Cu Kα1 line ($\lambda = 1.5406 \times 10^{-10}$ m).

3.2 X-ray rocking curve

X-ray rocking curve, tested by the High Resolution X-ray Diffractometer (D5005HR), was used to characterize the quality of the crystal. The rectangular sample used in this experiment was cut along its (010) direction, and the two faces perpendicular to the b direction were polished.

3.3 Effective segregation coefficients

The concentrations of elemental Nd, Gd, and Ca in the crystal were measured using an X-ray fluorescence spectrometer (Primus II) with which the relative standard deviation is less than 1%. The specimen measured was cut from the upper part of the as-grown boule. The polycrystalline material used for growing the crystal was referenced as the comparison standard. The segregation coefficients for Nd, Gd, Ca in the Nd^{3+}:CGB crystal would be calculated based on the measured results.

3.4 Density

Using the following equation, the density of 0.5 at.% Nd^{3+}:CGB crystal was calculated by the buoyancy method at room temperature (21.0°C).

$$\rho_{\exp} = \frac{m\rho_{\text{water}}}{m - m'}, \quad (1)$$

where m is the mass of the crystal sample in air, m' is the mass when it is immersed in water, and ρ_{water} is the density of water at the measurement temperature (ρ_{water} = 0.997 g/cm^3, 21.0°C).

3.5 Thermal properties

3.5.1 Thermal expansion determination

The average linear thermal expansion tensor components of Nd^{3+}:CGB was measured over the temperature range from 303.15 to 768.15 K using a thermal mechanical analyzer (Perkin Elmer model Diamond TMA). The sample used for the thermal expansion measurement was processed into a rectangular piece of dimensions 7.01 × 4.94 × 5.98 mm^3 ($a \times b \times c$). During the thermal expansion measurements, crystal samples were heated at a constant rate of 5 K min^{-1}, and the expansion ratio versus temperature curves along a, b and c directions were recorded.

3.5.2 Specific heat measurement

The specific heat was measured by using a differential scanning calorimeter (Diamond DSC). A small sample of the Nd^{3+}:CGB crystal (44.21 mg) was used in the specific heat measurement. The sample was held at 293.15 K for 15 min, heated to about 773.15 K at a constant rate of 10 K min^{-1} and then held at 773.15 K for 15 min to measure the specific heat. The specific heat was calculated using the supplied software of the equipment (Perkin–Elmer Co.).

3.5.3 Thermal diffusion coefficient measurements

The thermal diffusion coefficient of the Nd^{3+}:CGB single crystal was measured by the laser flash method using a laser flash apparatus (LFA457) over the temperature range 303.15–573.15 K. Three square wafers used for the measurements with the dimensions of [4.00 × 4.00 × 1.01 mm^3 ($a \times b \times c$), 4.00 × 4.00 × 1.01 mm^3 ($a \times c \times b$) and 4.00 × 4.00 × 1.00 mm^3 ($b \times c \times a$)] were coated by graphite on both sides. During the experiment, a short light pulse is used to heat the front surface of the wafer, and the temperature rise versus time on the opposite surface is measured using an IR detector. The thermal diffusivity coefficients can be calculated by using the analytical software provided (Netzsch Co.).

3.6 Spectra measurement

A cuboid with dimensions of 4 × 6 × 5 mm^3 ($a \times b \times c$) was cut from the grown crystal. All the surfaces of the sample were polished for spectral experiments. The polarized absorption spectra were measured at room temperature by a V-570 JASCO ultraviolet/visible/near infrared (UV/Vis/NIR) spectrophotometer. Scan speed was 60 nm/min and sampling interval was 0.5 nm.

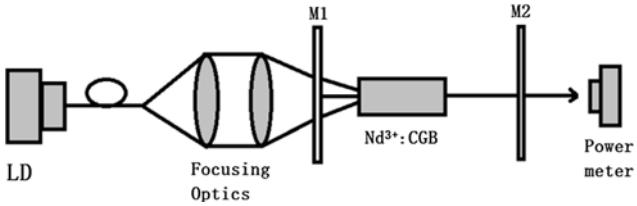

Fig. 2 Schematic diagram of the experimental laser setup

With the same sample that mentioned above, the polarized luminescence spectra and decay curve were also measured. Using the measured spectra, the optical intensity parameters were calculated through the J–O theory.

3.7 Laser performance

With the laser sample cut along b direction, CW laser operation was demonstrated by using a plano-concave resonator. The laser experimental setup is shown schematically in Fig. 2. The pump source was a fiber-coupled LD with the emission wavelength centered at 808 nm [15]. The output beam of the LD was focused onto the Nd^{3+}:CGB crystal sample with a spot radius of about 0.2 mm and a numerical aperture of 0.22 achieved by using a focusing lens. The length between M1 and M2 was about 22 mm. M1 was a plano mirror,antireflection (AR) coated at 808 nm on the pump face, high reflectance (HR) coated at 1.06 μm, and high-transmittance (HT) coated at 808 nm on the other face. The output coupler M2 was a concave mirror with a radius of curvature of 200 mm, and the output transmission is 2.0% at 1.06 μm. The sample was cut to the dimensions 4 × 5 × 6 mm^3 and the 4 × 5 mm^2 faces that perpendicular to its a direction were polished. During the experiments, the crystal was wrapped with indium foil and mounted on a copper block cooled by water. The cooling water was maintained at a temperature of 6°C.

4 Results and discussion

4.1 XRPD analysis of the Nd^{3+}:CGB crystal

X-ray powder diffraction (XRPD) analysis (with a scan speed of 0.2°/min) performed on the powdered reveals that it agrees well with the single phase CGB (Fig. 3), possessing a structure with *Pnma* space group. According to the peak 2θ values in the XRPD pattern, the Orthorhombic unit cell parameters are calculated to be a = 7.1908 Å, b = 15.5359 Å, and c = 8.6168 Å. These results are in close agreement with the data given in the JCPDS for CGB (a = 7.195 Å, b = 15.53 Å, and c = 8.619 Å) [16], the little difference is caused by Nd doping.

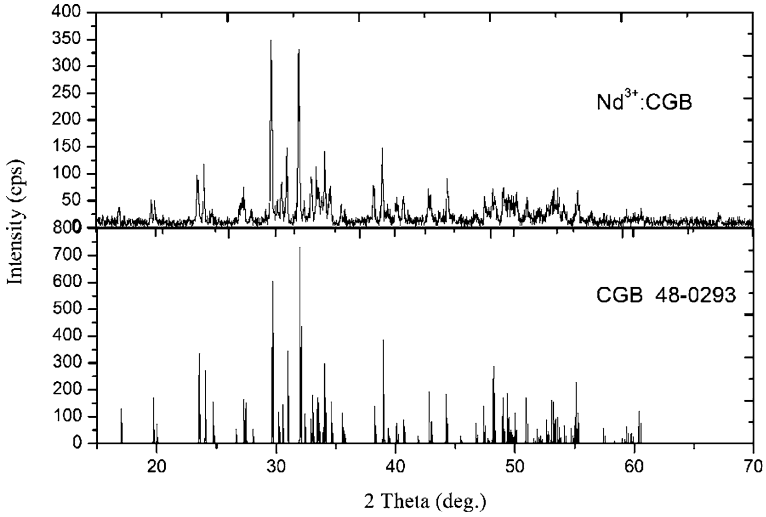

Fig. 3 XRPD patterns of the as-grown Nd^{3+}:CGB crystal and standard data

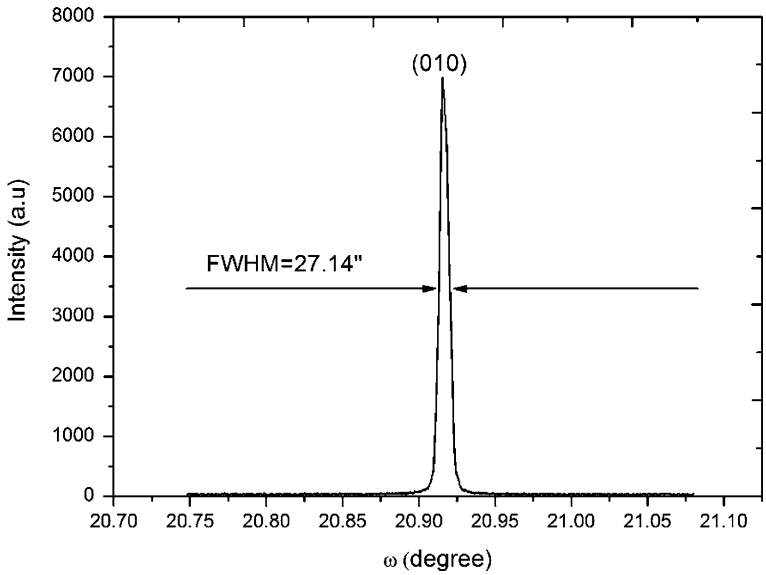

Fig. 4 X-ray rocking curves of the as-grown Nd^{3+}:CGB single crystal

4.2 X-ray rocking curve

Figure 4 shows the X-ray rocking curves corresponding to the (060) diffraction peak of the (010) crystal slabs. The full width at half-maximum (FWHM) values is only 27.14″. The diffraction peak show good symmetry without any splitting. These results indicate that the Nd^{3+}:CGB single crystal has highly perfect lattice structure and is suitable for laser applications and physical properties measurements.

4.3 Effective segregation coefficients

The effective segregation coefficients k of Nd^{3+}, Gd^{3+}, and Ca^{2+} in the Nd^{3+}:CGB crystal were calculated using the equation:

$$k = \frac{c_1}{c_2}, \tag{2}$$

Table 1 Effective segregation coefficients in Nd^{3+}:CGB crystal

	Standard (wt %)	Sample (wt %)	K_{eff}
Nd	0.215	0.229	1.06
Gd	46.718	46.299	0.99
Ca	17.950	18.212	1.01

where c_1 and c_2 are the respective concentrations of the ions in the crystal and raw materials. The results are shown in Table 1. The effective segregation coefficients of Nd^{3+}, Gd^{3+}, and Ca^{2+} were determined to be 1.06, 0.99, and 1.01, respectively. We found that the effective segregation coefficient of Nd^{3+} was a little higher than 1, which indicates that Nd^{3+} ions are comparative easily doped into this crystal,

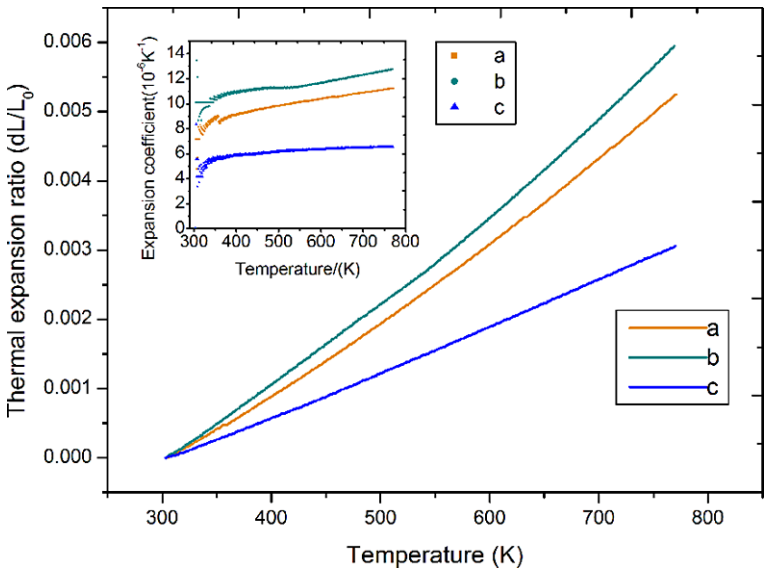

Fig. 5 Expansion ratio dL/L_0 and coefficient of Nd^{3+}:CGB measured along the a, b, c crystallographic directions

Table 2 Density of Nd^{3+}:CGB crystal

	Sample 1	Sample 2	Sample 3	Sample 4
m (g)	3.213	1.953	0.864	0.601
$m - m'$ (g)	0.694	0.423	0.187	0.130
ρ_{exp} (g/cm^3)	4.620	4.607	4.611	4.613
ρ_{av} (g/cm^3)			4.608	
ρ_{theory} (g/cm^3)			4.600	

and the Nd^{3+} concentration in the crystal is 0.53 at.% in the as-grown crystal.

4.4 Density

The theoretical density at room temperature was calculated by the following equation:

$$\rho = \frac{MZ}{N_A abc}, \tag{3}$$

where M is the molecular weight of the crystal, Z is the number of molecules in one unit cell, which is 4 for Nd^{3+}:CGB, N_A is the Avogadro's constant, and a, b, c are the lattice parameters, which were measured to be 7.202 Å, 15.559 Å, 8.634 Å, respectively. The density was calculated to be about 4.600 g/cm^3. By comparison, the buoyancy method measurements give an average experimental density of 4.608 g/cm^3 (Table 2), which is in good agreement with the calculated value.

4.5 Thermal properties

4.5.1 Thermal expansion of the Nd^{3+}:CGB crystal

The thermal expansion coefficient of a laser crystal is the one of the most important factors for the crystal growth and applications. The light absorption of a laser crystal causes a thermal gradient in a crystal that may disturb laser oscillation, and the thermal gradients can also lead to crystal fracture if they are high enough.

As we all know, the thermal expansion coefficient α_{ij} of a crystal is a symmetrical second-rank tensor [17]. Since the Nd^{3+}:CGB crystal belongs to the orthorhombic system, the two-fold axis lies along the crystallographic c-axis. The axes of both the principal and crystallographic coordinate systems have the same orientation, which can be expressed as $a//x1$, $b//x2$, $c//x3$. Based on Neumann's principle, there are three independent principal components. The respective average thermal expansion coefficient along the a-, b-, and c-axes can be obtained by measuring the thermal expansion of a-, b-, and c-oriented crystal samples [18]. Thermal expansion curves of Nd^{3+}:CGB versus temperature are shown in Fig. 5. The curves indicate that thermal expansion along a-, b- and c-directions are almost linear over the entire temperature range of 303.15–770.15 K.

The average thermal expansion coefficient can be calculated using the following equation:

$$\overline{\alpha}(T_0 \to T) = \frac{\Delta L}{L_0}\frac{1}{\Delta T}, \tag{4}$$

where $\overline{\alpha}(T_0 \to T)$ is the average thermal expansion coefficient over the temperature range from T_0 to T, L_0 is the sample length at T_0, ΔL is the length change when the temperature changes from T_0 to T, and the temperature change is $\Delta T = T - T_0$.

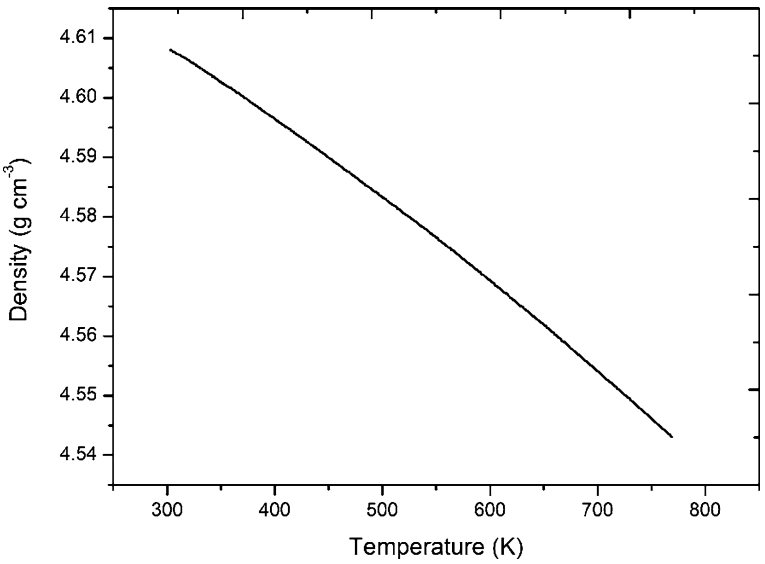

Fig. 6 Density variation in Nd^{3+}:CGB with temperature

A plot of the principal average thermal expansion coefficient components versus temperature from 25 to 500°C are shown in the upper left of Fig. 5. It can be calculated that the mean values of the average linear thermal expansion coefficients of a direction is 11.3×10^{-6}/K, b direction 12.6×10^{-6}/K and c direction 6.63×10^{-6}/K, respectively. We can see that the linear thermal expansion coefficient along the c direction is almost 2 times as larger than those along a or b direction. Thus, there is a considerable anisotropy in the thermal expansion of Nd^{3+}:CGB crystal. This implies that crystal of Nd^{3+}:CGB should be cooled down to room temperature at a low rate after the growth; otherwise cracks will easily occur inside the crystals. In our crystal-growing process, the cooling rate was chosen to be 20–30°C/h to obtain high-quality crystal.

4.5.2 Density versus temperature curve

The density of Nd^{3+}:CGB at different temperatures can be calculated using the following equation:

$$\rho = \frac{m}{abc} = \frac{m}{a_0 b_0 c_0} \frac{1}{(1+\frac{\Delta a}{a_0})(1+\frac{\Delta b}{b_0})(1+\frac{\Delta c}{c_0})} = \frac{\rho_0}{(1+\frac{\Delta a}{a_0})(1+\frac{\Delta b}{b_0})(1+\frac{\Delta c}{c_0})} \quad (5)$$

where $\rho_0 = 4.608\ \mathrm{g\,cm^{-3}}$ is the density of the crystal at T_0 of 294.15 K, and the values of $\Delta a/a_0$, $\Delta b/b_0$ and $\Delta c/c_0$ can be obtained from the expansion ratios in Fig. 5. The density versus temperature curve of the crystal over the temperature range from 303.15 to 770.15 K is shown in Fig. 6.

4.5.3 Specific heat capacity

Specific heat is one of the most important thermal factors in the laser crystals that influences the damage threshold of a crystal. Generally, the crystal with high specific heat possesses a large damage threshold. Figure 7 shows the specific heat versus temperature curve of the Nd^{3+}:CGB crystal measured by differential calorimetry. It can be seen that the specific heat of the crystal increases from 0.498 to 0.679 $\mathrm{J\,g^{-1}\,K^{-1}}$ as the temperature rises from 293.15 to 573.15 K. The specific heat of Nd^{3+}:CGB crystal is 0.498 $\mathrm{J\,g^{-1}\,K^{-1}}$ (79.67 $\mathrm{cal\,mol^{-1}\,K^{-1}}$) at 330 K. In comparison with Nd^{3+}:YCOB (82.4 $\mathrm{cal\,mol^{-1}\,K^{-1}}$) and Nd^{3+}:YVO_4 (24.6 $\mathrm{cal\,mol^{-1}\,K^{-1}}$) crystals [19], Nd^{3+}:CGB crystal has relative large specific heat. Since the Nd^{3+}:YCOB and Nd^{3+}:YVO_4 crystals both have high optical damage threshold [20], it can be indicated that Nd^{3+}:CGB crystal should have high damage threshold.

4.5.4 Thermal diffusion coefficient

The thermal diffusion coefficient a_{ij} of the crystal is also a symmetrical second-rank tensor similar to the thermal expansion coefficient. It has three independent principal components, which can be obtained by the measurement of the sample cut along a, b, and c direction. The results are shown in Fig. 8. It can be seen that the thermal diffusivity decrease slowly with increasing temperature. At 303 K, the thermal diffusivity along the a-axis is 0.36 $\mathrm{mm^2/s}$, and the b-axis and c-axis are 0.376 $\mathrm{mm^2/s}$, 0.358 $\mathrm{mm^2/s}$, respectively. It can be seen that there has relatively low anisotropy among the three directions.

4.5.5 Thermal conductivity

The thermal conductivity of Nd^{3+}:CGB was calculated using the results of thermal diffusivity measured by the laser

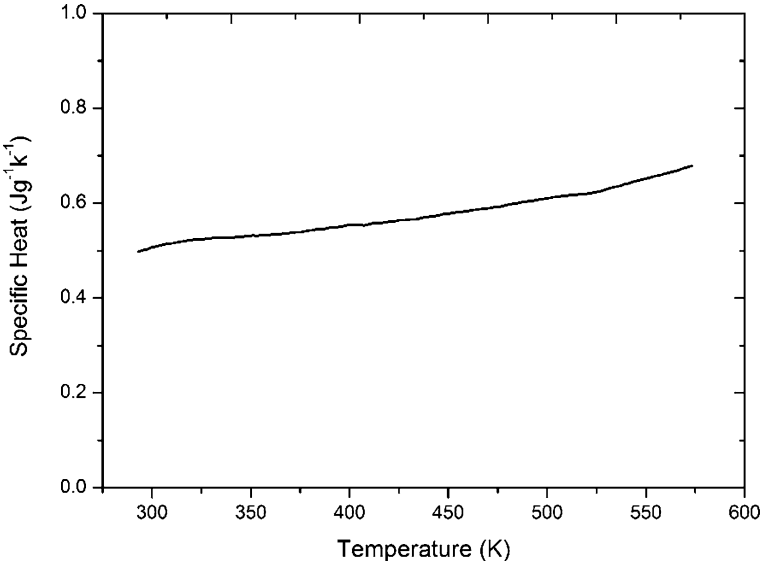

Fig. 7 The specific heat versus temperature curve of the Nd^{3+}:CGB crystal

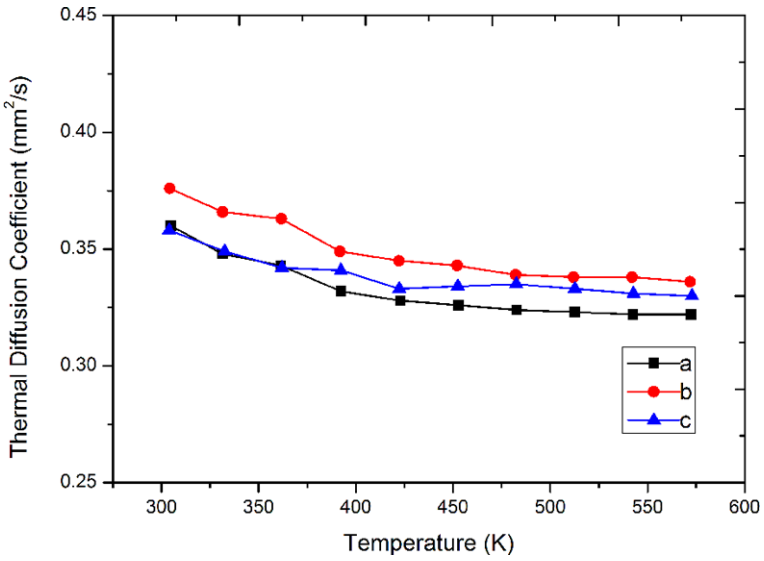

Fig. 8 Thermal diffusivity variation in Nd^{3+}:CGB with temperature

flash method and the specific heat data according to the following equation:

$$k = \lambda \rho C_p, \tag{6}$$

where λ, C_p, and ρ denote the thermal diffusivity, specific heat and density of the Nd^{3+}:CGB crystal, respectively. The obtained thermal conductivity of Nd^{3+}:CGB along different directions is plotted in Fig. 9.

It can be seen that the thermal conductivity of Nd^{3+}:CGB increases with rising temperature, a behavior that is not typical of most crystals. The thermal conductivity of Nd^{3+}:CGB along the *a*-, *b*-, and *c*-axis are 0.849, 0.887, and 0.841 $W\,m^{-1}\,K^{-1}$ at room temperature, respectively. Compared with other crystals, the thermal conductivity of Nd^{3+}:CGB crystal is relatively small. Thus, there is a limit in the high power laser operation.

We know that the thermal conductivity of glasses increases with increasing temperature, whereas for crystalline substances it decreases with increasing temperature. Figure 9 shows that the thermal conductivity of Nd^{3+}:CGB is similar to the glasses behavior. The behavior of Nd^{3+}:CGB should possibly be related to the disorder structure of the crystal. Namely, Ca^{2+} and Gd^{3+} ions are statistically situated in three different sites in the Nd^{3+}:CGB crystal structure [12].

The thermal conductivity can also be written as

$$k = \frac{1}{3}\rho C_p v L, \tag{7}$$

where ρ is the density, which decreases by only 1.41% from 303.15 to 769.15 K (Fig. 6), v is the sound velocity, which is considered as a constant [21], C_p is the specific heat of the crystal (Fig. 7), and L is the phonon mean free path.

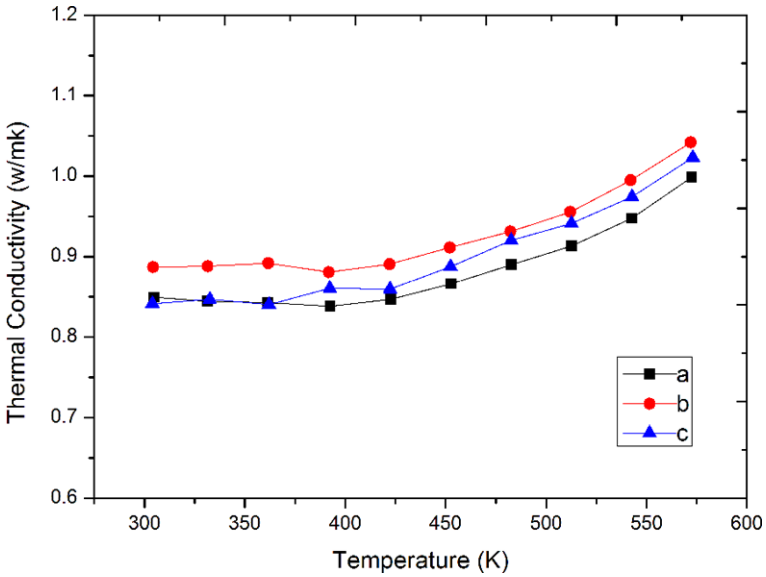

Fig. 9 Thermal conductivity variation in Nd^{3+}:CGB with temperature

Generally, the numerical value of L in a perfect crystal mainly depends on the magnitude of the anharmonic interactions, and also on the total density of phonon. When the crystal is heated, interactions between the phonons increase, which in turn leads to the reduction in the phonon mean free path, and correspondingly, to a decrease in the thermal conductivity with increasing temperature.

In the case of Nd^{3+}:CGB, not only the anharmonic interactions are responsible for establishing the thermal equilibrium among the phonons, but also the mean free path L is also related to the disordered nature of the crystal structure. So, if we take an extreme case that the disordered structure completely determines the phonon mean free path L, the value of L could be considered as a constant [22, 23]. Thus, the thermal conductivity k changes mainly due to the changing specific heat, a factor that increases with increasing temperature.

4.6 Spectroscopic characteristics

Figure 10 shows the absorption spectra of Nd^{3+}:CGB crystal measured at room temperature. E represents the electric field direction of the incident light. Figure 11 shows the absorption cross sections in the region of 720–910 nm for clarity. Obviously, the polarized spectra help us to get a better understanding of the optical properties of Nd^{3+}:CGB compared with the previous unpolarized spectra [9, 24]. It shows that the absorption for $E//c$ is the strongest one among the three directions, and the peak absorption cross-section at 805 nm is about 3.312×10^{-20} cm^2 with the broad bandwidth (FWHM) about 15 nm. Therefore, the $E//c$ polarized direction can be treated as the most effective pump direction. For $E//a$ and $E//b$ polarizations maximal absorption cross sections near 805 nm are 2.669×10^{-20} cm^2 and

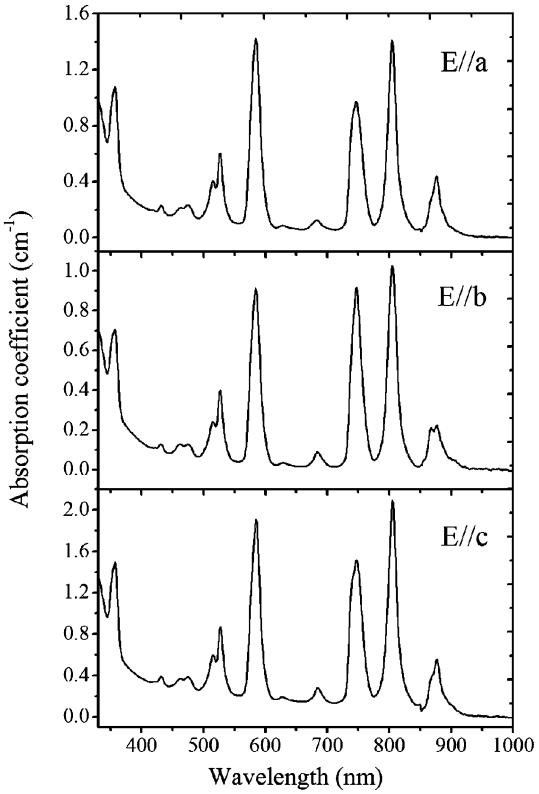

Fig. 10 Polarized absorption spectra of the 0.53 at.% Nd^{3+}:CGB crystal

2.824×10^{-20} cm^2, and the broad bandwidth (FWHM) are 15 nm and 16 nm, respectively. This broad bandwidth means that Nd^{3+}:CGB is more suitable for diode pumping and indicates an inhomogeneous broadening behavior [25], which is probably due to the structural disorder of Nd^{3+}:CGB crystal. The Judd–Ofelt (J–O) theory [26, 27] is applied to analyze the room-temperature absorption spectra. Since Judd

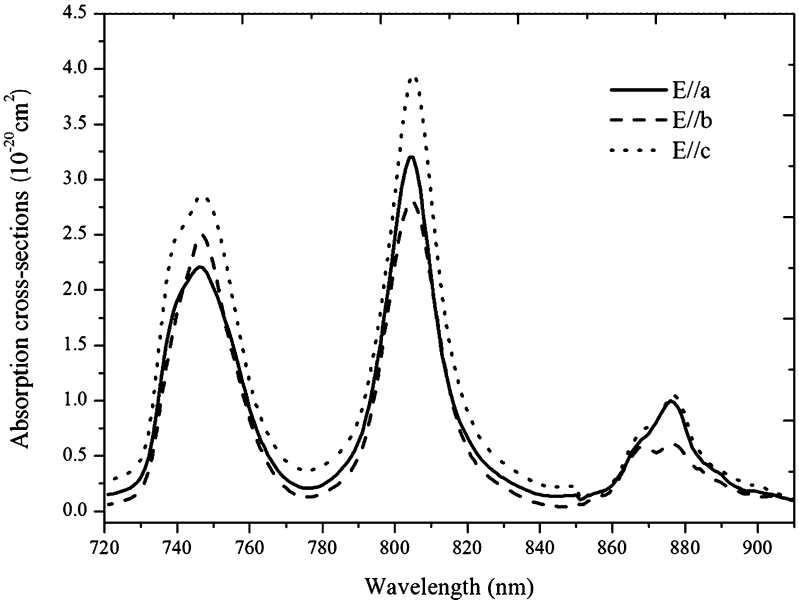

Fig. 11 Polarized absorption cross sections of the 0.53 at.% Nd^{3+}:CGB crystal in a range of 720–910 nm

Table 3 Experimental transition-line intensity parameters and oscillator strength of the polarized absorption spectrum of Nd^{3+}:CGB crystal

Transition final state $4f^n\psi' J'$	$E//a$		$E//b$		$E//c$	
	$S_{exp}(J \to J')$ (10^{-20} cm^2)	$P_{exp}(J \to J')$ (10^{-6})	$S_{exp}(J \to J')$ (10^{-20} cm^2)	$P_{exp}(J \to J')$ (10^{-6})	$S_{exp}(J \to J')$ (10^{-20} cm^2)	$P_{exp}(J \to J')$ (10^{-6})
$^4D_{1/2}$	2.93	13.4	1.43	12.60	3.20	14.63
$^4P_{1/2}$	0.18	0.68	4.57	0.63	0.25	0.95
$^4G_{11/2}$	0.6	2.05	4.51	2.13	0.66	2.27
$^4G_{9/2}$	1.12	3.48	0.36	3.41	1.19	3.68
$^4G_{5/2}$	5.64	15.8	5.35	15.01	5.71	15.98
$^4F_{9/2}$	0.24	0.58	1.1	0.87	0.38	0.91
$^4S_{3/2}$	3.59	7.87	0.62	9.89	4.43	9.70
$^2H_{9/2}$	3.85	7.85	0.17	9.30	4.85	9.85
$^4F_{3/2}$	1.19	2.22	2.75	2.66	1.4	2.62

Table 4 Judd–Ofelt intensity parameters of Nd^{3+} in CGB crystal

Intensity parameters ($\Omega \times 10^{-20}$ cm^2)	$E//a$	$E//b$	$E//c$	Effective
Ω_2	2.51	2.18	2.17	2.29
Ω_4	7.27	7.12	7.94	7.44
Ω_6	7.01	9.29	8.83	8.38

and Ofelt published their papers in 1962, the J–O theory and its extension have become the most popular method in the analysis of spectroscopic properties of rare earth ions doped crystals and glasses. Thus, only the calculation results are presented and the detailed calculation procedure is similar to that reported in [4]. The reduced matrix element of unit tensor operators used in the fitting can be found in [28]. The refractive index used for the calculation was roughly taken as 1.77 [29]. The measured transition-line intensity and oscillator strength, denoted by S_{exp} and P_{exp}, respectively, are listed in Table 3. The calculated J–O intensity parameters Ω_t ($t = 2, 4, 6$) are listed in Table 4. For the biaxial crystal, the effective J–O intensity parameters are defined as [30] and their values are also listed in Table 4. Table 5 shows Ω_t ($t = 2$, 4 and 6) values for Nd^{3+}:CGB crystal obtained in this work, and makes comparison with the same parameters for other Nd-doped crystals. As a rule, the value of intensity parameter Ω_2 depends on the structure and the symmetry of

Table 5 Comparison of Judd–Ofelt parameters for Nd^{3+}:CGB with other Nd-doped crystals

Crystals	$\Omega_2 \times 10^{-20}$ cm^2	$\Omega_4 \times 10^{-20}$ cm^2	$\Omega_6 \times 10^{-20}$ cm^2	X	Reference
Nd^{3+}:CGB	2.29	7.44	8.38	0.89	(This work)
	4.59	7.56	10.76	0.7	[9]
Nd^{3+}:$SrGdGa_3O_7$	1.88	4.44	2.96	1.5	[4]
Nd^{3+}:YAG	0.2	2.7	5.0	0.54	[31]
Nd^{3+}:GGG	0.02	6.7	6.7	1	[32]
	0	3.3	3.7	0.89	[31]
Nd^{3+}:YAP	0.69	3.69	4.56	0.81	[33]

Table 6 Luminescence parameters of Nd^{3+}:CGB for the radiative ${}^4F_{3/2} \rightarrow {}^4I_{J'}$ transition

Final state	$E//a$				$E//b$				$E//c$			
	$S_{cal}(J'' \rightarrow J')$ (10^{-20} cm^2)	$A(J'' \rightarrow J')$ (s^{-1})	$\beta_{J''J}$ (%)	$\sigma_e(\lambda)$ (10^{-20} cm^2)	$S_{cal}(J'' \rightarrow J')$ (10^{-20} cm^2)	$A(J'' \rightarrow J')$ (s^{-1})	$\beta_{J''J}$ (%)	$\sigma_e(\lambda)$ (10^{-20} cm^2)	$S_{cal}(J'' \rightarrow J')$ (10^{-20} cm^2)	$A(J'' \rightarrow J')$ (s^{-1})	$\beta_{J''J}$ (%)	$\sigma_e(\lambda)$ (10^{-20} cm^2)
${}^4I_{9/2}$	2.07	2593.97	41.54	0.84	2.16	2718.7	37.36	1.03	2.32	2924.5	39.75	1.08
${}^4I_{11/2}$	3.89	3040.98	48.7	3.53	4.79	3749.63	51.52	4.35	4.72	3663.67	49.8	4.28
${}^4I_{13/2}$	1.49	581.59	9.31	1.45	1.97	772.38	10.61	1.81	1.87	734.25	9.98	1.31
${}^4I_{15/2}$	0.20	27.69	0.44		0.26	36.69	0.50		0.25	34.88	0.47	

coordination of a crystal. Generally, the higher the value of Ω_2 the larger component of covalent bond of the compound contains, that is if the crystal has a relative high value of Ω_2, the crystal would present the glass behavior. From Table 5, one can conclude that Nd^{3+}:CGB has a large component of covalent bond because of its high value of Ω_2. Thus, we can conclude that Nd^{3+}:CGB shows the glass behavior which is in agreement with the disordered structure of the crystal on the other hand. In addition, we know that the value of the parameter Ω_2 has no practical effect on the emission properties of the crystal from the ${}^4F_{3/2}$ state, as they mainly depend on the parameters Ω_4 and Ω_6. The spectroscopic quality parameter $X = \Omega_4/\Omega_6$ is 0.89, which is less than 1 and this indicates that the emission to the ${}^4I_{11/2}$ manifold is the more feasible than that to the ${}^4I_{9/2}$ manifold.

On the basis of the calculated J–O intensity parameters, the radiative transition rates $A(J'' \rightarrow J')$, fluorescent branching ratio $\beta_{J''J}$ of Nd^{3+}:CGB crystal could be calculated and the results with three polarized directions are listed in Table 6. Here, one can find that the branching ratio of ${}^4F_{3/2} \rightarrow {}^4I_{11/2}$ with $E//b$ and $E//c$ are almost have the same value which are both bigger than the branching ratio with $E//a$. Combining with the larger absorption cross section at 805 nm for $E//c$, polarized and more efficient 1.06 µm laser output may be realized in a a- or b-cut Nd^{3+}:CGB crystal.

Radiative lifetime τ_{rad} of ${}^4F_{3/2}$ manifold is the reciprocal of the total spontaneous emission probabilities from the manifold. For anisotropic crystal, the total spontaneous emission probability is given as

$$A_{Total}(J'') = \frac{\sum_q \sum_{J'} A(J'' \rightarrow J')}{3} \tag{8}$$

So, the radiative lifetime of the ${}^4F_{3/2}$ manifold for the Nd^{3+} in CGB crystal is estimated to be 143.68 µs. Fluorescence decay curve of the Nd^{3+}:CGB crystal is shown in Fig. 12. By linear fitting, the fluorescence lifetime could be obtained to be 116.3 µs, so the radiative quantum efficiency of the ${}^4F_{3/2}$ manifold is $\eta = 116.3/143.68 = 80.94\%$. The results indicate that Nd^{3+}:CGB crystal can be considered as a promising material for solid-state laser application.

The stimulated emission cross section σ_e can be calculated from

$$\sigma_e = \frac{\lambda_p^2}{4\pi^2 n^2 \Delta\nu} A, \tag{9}$$

where $\Delta\nu$ is the frequency of full width at half maximum (FWHM), λ_p is the wavelength of the fluorescent peak and A is the radiative transition rate. Figure 13 shows the polarized emission spectra with three different directions and the emission cross-section values at peak fluorescence wavelengths are listed in Table 6. The peak wavelength of fluorescence spectrum for $E//c$ is located at 1065 nm and differs from those for $E//a$ and $E//b$, which shift to 1062 nm, though the FWHMs at peak wavelength for different polarized directions have the same value of 30 nm. Such a large bandwidth shows that Nd^{3+}:CGB may possibly be used in laser systems to produce femtosecond pulses [34]. The inhomogeneous broadening of the Nd^{3+} lines is attributed to

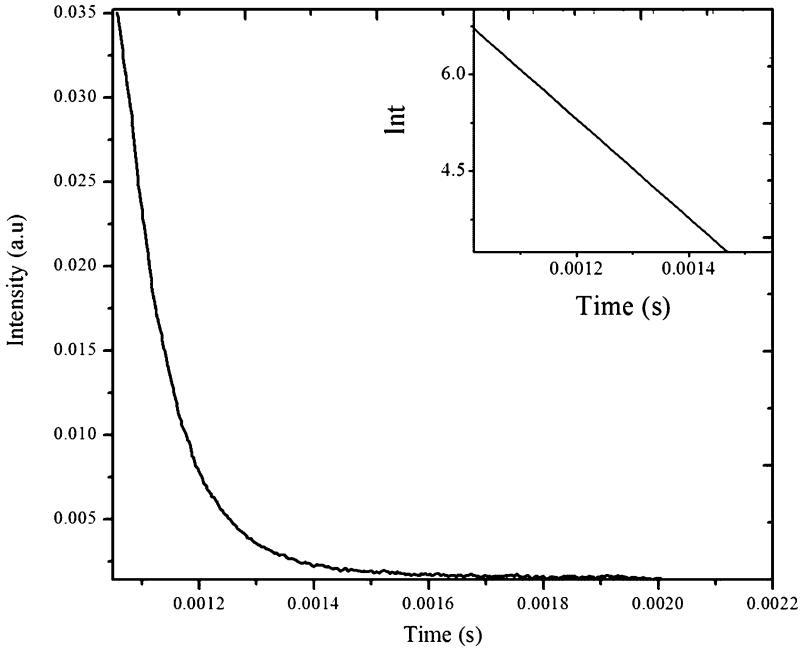

Fig. 12 Fluorescence decay curve and linear fitting curve of Nd^{3+}:CGB crystal recorded at 1062 nm under 808 nm excitation

the variation of the local crystal field surrounding the Nd^{3+} ions resulting from the high degree of structural disorder that Nd^{3+}, Ca^{2+}, and Gd^{3+} ions are statistically situated in three different sites in the Nd^{3+}:CGB crystal structure. From Table 6, we can find that the emission cross-section values for three polarized directions at 1.06 μm are all smaller than that of 4.00 at.% Nd^{3+}:$GdAl_3(BO_3)_4$ (63.0×10^{-20} cm^2) [35]. Combing the relative longer fluorescence lifetime, it can be indicated that Nd^{3+}:CGB should have a higher energy storage capacity in the Q-switched laser operation process.

4.7 Laser performance

The continuous-wave (CW) laser performance at 1.06 mm was demonstrated for the first time. The output powers under various incident powers were measured using a power meter, and the results are shown in Fig. 14. The pumping threshold of Nd^{3+}:CGB crystal is 1.37 W, the highest output power of 603 mW at 1.06 μm was achieved at a pumping power of 7.24 W, the optical-to-optical conversion efficiency is 8.33%, and the slope efficiency of 9.55% is thus calculated from the linear part of the curve. It can be found from Fig. 14 that the output power was not saturated when the incident power was 7.24 W, so higher output power may be achieved when the pump power increases. In addition, the sample used in the laser experiment was not coated and only one output couple with transmission of 2.0% was used in the experiment. Therefore, more efficient laser output may be realized if the sample and the transmission of the output couple are optimized. With a spectrum analyzer, the laser spectrum was recorded, and is shown in the upper left of Fig. 14. From Fig. 14, it can be seen that the laser band is centered at 1069 nm.

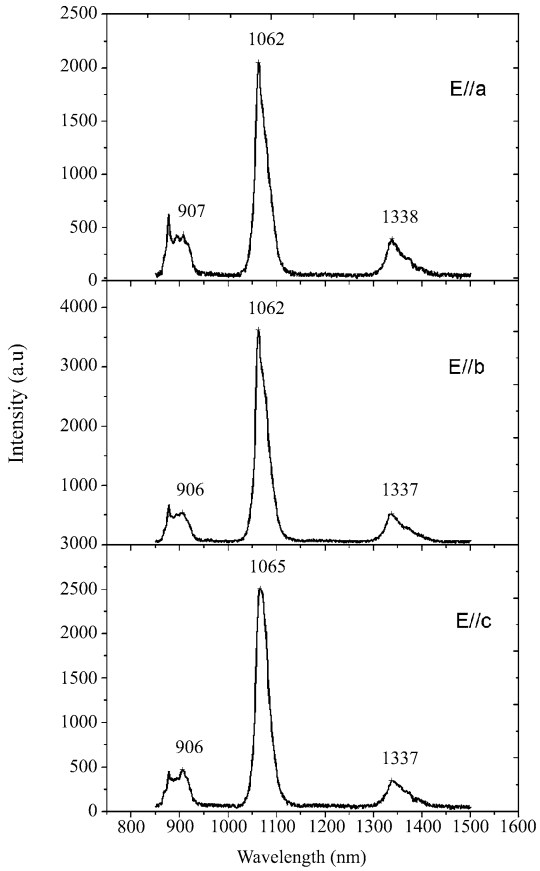

Fig. 13 Polarized emission spectra of the 0.53 at.% Nd^{3+}:CGB crystal

5 Conclusions

A Nd^{3+}:CGB laser crystal was grown by the Czochralski method. Several thermal, optical, and laser properties were

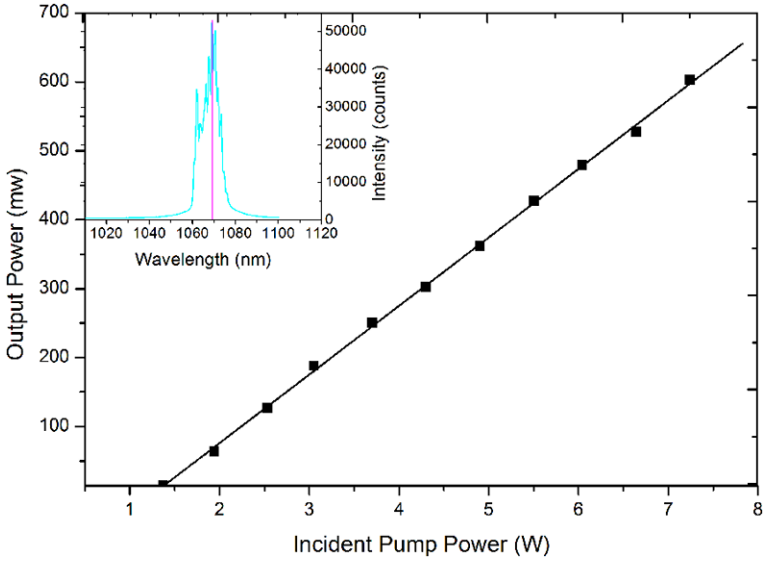

Fig. 14 Average output power versus incident pump power. Insert: spectrum of Nd^{3+}:CGB

measured. The effective segregation coefficient of Nd^{3+} was determined to be 1.06. The results show that the thermal conductivity of Nd^{3+}:CGB increases with increasing temperature, which indicates the glass-like behavior of the crystal. Polarized absorption spectra, polarized fluorescence spectrum and fluorescence decay curve of the Nd^{3+}:CGB crystal were measured. The results show that the absorption and emission spectra of Nd^{3+} are inhomogeneously broadened, which is attributed to the disordered structure. Based on J–O theory, the anisotropy of the spectral properties for different polarized directions was discussed. The broad emission spectra shows that Nd^{3+}:CGB may possibly be used in laser systems to produce femtosecond pulses. LD-end-pumped CW laser operation at 1.06 μm was demonstrated for the first time. A maximum power of 603 mW was obtained with an optical conversion efficiency of 8.83% and slope efficiency of 9.95%. Therefore, All of these properties show that Nd^{3+}:CGB is a promising disordered crystalline laser material.

Acknowledgements This work was supported by the National Natural Science Foundation of China (Grant Nos. 51025210 and 51021062), the National Basic Research Program of China (Grant No. 2010CB630702), and the Program of Introducing Talents of Discipline to Universities in China (111 program).

References

1. G.Q. Xie, D.Y. Tang, W.D. Tan, H. Luo, H.J. Zhang, H.H. Yu, J.Y. Wang, Opt. Lett. **34**, 103 (2009)
2. G.Q. Xie, D.Y. Tang, H. Luo, H.J. Zhang, H.H. Yu, J.Y. Wang, X.T. Tao, M.H. Jiang, L.J. Qian, Opt. Lett. **33**, 1872 (2008)
3. T.T. Basiev, N.A. Es'kov, A.Ya. Karasik, V.V. Osiko, A.A. Sobol, S.N. Ushakov, M. Helbig, Opt. Lett. **17**, 201 (1992)
4. Y.Y. Zhang, H.J. Zhang, H.H. Yu, J.Y. Wang, W.L. Gao, M. Xu, S.Q. Sun, M.H. Jiang, R.I. Boughton, J. Appl. Phys. **108**, 063534 (2010)
5. O.A. Aliev, P.F. Pza-Zade, L.R. Shakhalieva, Sci. Pap. Azerb. State Univ., Ser. Khim. **4**, 18 (1970)
6. B.F. Dzhurinski, I.V. Tananaev, O.A. Aliev, Izv. Ak. Nauk SSSR, Neorg. Mater. **4**, 1972 (1968)
7. B.F. Dzhurinski, O.A. Aliev, I.V. Tananaev, Izv. Ak. Nauk SSSR, Neorg. Mater. **6**, 1592 (1970)
8. Y. Zhang, Z.B. Lin, Z.S. Hu, G.F. Wang, J. Solid State Chem. **177**, 3183 (2004)
9. B.V. Mill, A.M. Tkachuk, E.L. Belokoneva, G.I. Ershova, D.I. Mironov, I.K. Razumova, J. Alloys Compd. **275**, 291 (1998)
10. Z. Burshtein, Y. Shimony, I. Levy, A.M. Lejus, J.M. Benitez, F. Mougel, J. Opt. Soc. Am. B **13**, 1941 (1996)
11. A.V. Terentiev, P.V. Prokoshin, K.V. Yumashev, V.P. Mikhailov, W. Ryba-Romanowski, S. Golab, W. Pisarski, Appl. Phys. Lett. **67**, 2442 (1995)
12. C.Y. Tu, Y. Wang, Z.Y. You, J.F. Li, Z.J. Zhu, B.C. Wu, J. Cryst. Growth **265**, 154 (2004)
13. H.J. Zhang, H.D. Jiang, J.Y. Wang, X.B. Hu, G.W. Yu, W.T. Yu, L. Gao, J.A. Liu, S.J. Zhang, M.H. Jiang, Appl. Phys. A **78**, 889 (2004)
14. H.D. Jiang, J.Y. Wang, H.J. Zhang, X.B. Hu, H. Liu, Opt. Mater. **23**, 461 (2003)
15. Y.G. Yu, J.Y. Wang, H.J. Zhang, Z.P. Wang, H.H. Yu, M.H. Jiang, Opt. Lett. **34**, 467 (2009)
16. S. Ivanov, V.Ya.L. Zhurov, Karpov Inst. of physical Chemistry, Moscow, Russia, ICDD Grant-in-Aid, 1996
17. J.F. Nye, *Physical Properties of Crystals* (Oxford University Press, Oxford, 1985)
18. W.W. Ge, H.J. Zhang, J.Y. Wang, J.H. Liu, X.G. Xu, X.B. Hu, M.H. Jiang, D.G. Ran, S.Q. Sun, H.R. Xia, R.I. Boughton, J. Appl. Phys. **98**, 013542 (2005)
19. C.Q. Wang, H.J. Zhang, X.L. Meng, L. Zhu, Y.T. Chow, X.S. Liu, R.P. Cheng, Z.H. Yang, S.J. Zhang, L.K. Sun, J. Cryst. Growth **220**, 114 (2000)
20. H.J. Zhang, L. Zhu, X.L. Meng, Z.H. Yang, C.Q. Wang, W.T. Yu, Y.T. Chow, M.K. Lu, Cryst. Res. Technol. **34**, 1011 (1999)
21. C.L. Choy, W.P. Leung, T.G. Xi, Y. Fei, C.F. Shao, J. Appl. Phys. **71**, 170 (1992)
22. C. Kittel, Phys. Rev. **75**, 972 (1949)
23. C.L. Choy, W.P. Leung, T.G. Xi, Y. Fei, C.F. Shao, J. Appl. Phys. **71**, 170 (1992)
24. Y. Wang, C.Y. Tu, Z.Y. You, J.F. Li, Z.J. Zhu, G.H. Jia, X.A. Lu, B.C. Wu, J. Mod. Opt. **53**, 1141 (2006)

25. W.F. Krupke, Phys. Rev. **145**, 325 (1966)
26. B.R. Judd, Phys. Rev. **127**, 750 (1962)
27. G.S. Ofelt, J. Chem. Phys. **37**, 511 (1962)
28. W.T. Carnall, P.R. Fields, K. Rajnak, J. Chem. Phys. **49**, 4424 (1968)
29. P.H. Haumesser, R. Gaume, B. Viana, D. Vivien, J. Opt. Soc. Am. B **19**, 2365 (2002)
30. Z. Luo, X. Chen, T. Zhao, Opt. Commun. **134**, 415 (1997)
31. E. Cavalli, E. Zannoni, A. Belletti, V. Carozzo, A. Toncelli, M. Tonelli, M. Bettinelli, Appl. Phys. B **68**, 677 (1999)
32. A.A. Kaminskii, *Crystalline Lasers: Physical Processes and Operating Schemes* (CRC Press, New York, 1996)
33. H. Zhang, Z. Luo et al., Chin. J. Infrared Res.. Ser. A, Chin. Ed. **7**, 297 (1998)
34. A.A. Kaminskii, *Laser Crystals* (Springer, Berlin, 1981)
35. Y. Zhang, Z.b. Lin, Z.S. Hu, G.F. Wang, J. Solid State Chem. **177**, 3183 (2004)